



Effect of quenching rate on fatigue crack growth of hypereutectoid rail steel

Yaodong Cen¹, Lin Chen^{1,*}, Rui Dong¹, and Qingfei Zhou¹

¹School of Materials and Metallurgy, Inner Mongolia University of Science and Technology, Baotou 014010, China

Received: 23 February 2020

Accepted: 9 July 2020

Published online:
27 July 2020

© Springer Science+Business Media, LLC, part of Springer Nature 2020

ABSTRACT

Fatigue damage of rail steel is an important issue affecting economic and human safety. In this paper, the effect of different quenching rates on the fatigue crack growth of hypereutectoid rail is analyzed. The material parameters C and m of the Paris formula are measured. The results show that an increase in cooling rate of rail decreases the value Paris law parameter C , increases the value m and decreases fatigue crack growth rate. This can be attributed to the decreased in the lamellar spacing and cluster diameter of the pearlite with an increase in cooling rate. More specifically, the smaller lamellar spacing and the cluster diameter make the crack pass easily through the cluster boundary of pearlite, which increases the number of zigzag crack growth paths and branching cracks that can help restrain fatigue crack growth. The fatigue fracture characteristic of hypereutectoid rail is that with an increase in cooling rate, the fatigue striation spacing and river pattern of the fracture surface become smaller, the crack growth path tends to zigzag, the tearing edges become deeper and the surface is relatively rougher.

Introduction

The continuous increase in train speed has led to an increasingly more complex rail service environment in which rail steel plays an important role in railway transportation. Fatigue growth resistance is a key indicator to evaluate the service life of heavy-duty rail [1–3]. As hypereutectoid rail with an 0.8% carbon content is cooled slowly from a high temperature, a pearlite structure can be obtained. However, the grain structure is coarse and the toughness is poor [4]. It has been proved that optimizing quenching process to obtain a fine pearlite structure is an

effective way to improve fatigue performance of rail [5]. Zhou et al. [6] studied the influence of carbon content, the heat treatment parameters and microstructure of rail and determined that refining the pearlite lamellar spacing structure of rail is the most effective way to achieve high strength and toughness. Gong et al. [7] found that coarse pearlite lamellar spacing will reduce the fracture toughness. Further studies include the effect of microstructure on the fatigue crack growth rate. Akama et al. [8] proposed a long coplanar I/II/III fatigue crack growth model of rail under a non-proportional mixed mode load, proposed the equivalent stress intensity

Address correspondence to E-mail: 465378809@qq.com

factor range considering the crack surface contact and successfully regressed the growth rate data of secondary crack.

Jones et al. [9] studied the relationship between da/dN and ΔK of short cracks in the process of fatigue crack growth and also discussed how to use the existing equation to predict the growth of short cracks and explain the crack growth path. Gao et al. [10] studied the crack initiation and propagation of U71Mn rail and determined that inclusion and stress concentration had a great influence on fatigue crack propagation. However, most of the above research has focused on the influence of structure, fatigue crack growth rate and fatigue failure. How to control the rail cooling rate, given sufficient pearlite development time, and obtain the optimal pearlite structure and lamellae have rarely been reported. The previous systematic research on the effect of pearlite lamellar spacing of U75V heavy rail steel on a fatigue crack growth path found that increasing the deflection path of the crack can enhance the blocking effect of the crack growth, which is conducive to restrain fatigue crack growth [11, 12].

Based on the previous works, this paper further studies the fatigue crack growth behavior of hypereutectoid rail under different quenching rates, compares and analyzes the resulting fatigue crack growth performance, clarifies the relationship between microstructure, lamellar spacing, fatigue striation spacing and the crack growth of high-carbon rail, and provides a theoretical basis for the production of high-performance hypereutectoid rail in the transportation industry.

Materials and method

Hypereutectoid rail was selected as the experimental material; the chemical composition of materials is listed in Table 1. The samples of hypereutectoid rail were quenched from 860 to 20 °C at different cooling rates as listed in Table 2. The austenite temperature of the sample was recorded using a SONY-F4.5GM thermal imager as shown in Fig. 1. According to the technical conditions for *Ordering 45 ~ 75 kg/m rails (TB/T 2344-2012)*, a compact tensile (CT) specimen was used for crack propagation testing. The specimen was taken from the position of a 75 kg/m hypereutectoid rail head, and the sampling position is shown in Fig. 2a. The size of the CT specimen is according to

GB/T6398-2000 as shown in Fig. 2b. The CT specimens were polished and etched with 4% nitric acid alcohol prior to the crack propagation testing. The fatigue crack growth test was carried out using SIN-COTEC high-frequency fatigue testing machine as shown in Fig. 2c. For the fatigue test, a 50 Hz sine wave waveform was applied. The crack length a corresponding to the number of cycles was measured by the visual method in which a convenient microscope with magnification of 20–50 times was used according to the *GB/T6398-2000*. The applied maximum load was 8 kN, the minimum load was 4 kN, and the stress ratio was $R = 0.5$.

The lamellar spacing of the pearlite structure of hypereutectoid rail was measured by Image Pro-Plus 6.0 software. The crack growth track and morphology were observed using a Zeiss metallographic microscope. The Brinell hardness test using HBW5/750/10 was carried out at six different positions on both sides of the crack as shown in Fig. 2d, and then, the average value was calculated. The fatigue fracture surface was cleaned with acetone ultrasonic, and the fracture morphology was observed using a Quantum-400 scanning electron microscope. The fatigue striation spacing was measured using Image J software.

$a-N$ curve analysis of fatigue crack growth

The measured crack length a and number of cycles N of the CT with different cooling rates of hypereutectoid rail are listed in Table 3. The $a-N$ curve is obtained by measuring a and N as shown in Fig. 3. Figure 3 shows that the general trend is that the crack propagation rate decreases with an increase in the cooling rate. The $a-N$ curve trend of rails with cooling rates of 1 °C/s, 2 °C/s and 3 °C/s is basically similar, indicating that the fatigue crack growth performance of hypereutectoid rails with cooling rates of 2 °C/s and 3 °C/s is not significantly improved compared with that of 1 °C/s. However, the crack growth curve of 5 °C/s and 8 °C/s samples is gentle at the initial stage and then starts to steep after point A and point B. The reason for the great fatigue property improvement is that: The pearlite transition temperature decreases rapidly with an increase in the cooling rate; the pearlite lamellar spacing is refined; the thickness of ferrite and cementite is thinner; and the phase interface is increased, while the phase interface can block the dislocation movement and it needs

Table 1 Chemical composition of materials (wt%)

Material	C	Mn	P	S	Cr	Nb	RE	Si
Hypereutectoid rail	0.820~0.856	0.966	≤ 0.025	≤ 0.015	0.465~0.537	0.012~0.019	0.0015	0.70

Table 2 Rail quenching process parameters

Material	Process conditions				
	1 (°C/s)	2 (°C/s)	3 (°C/s)	5 (°C/s)	8 (°C/s)
Hypereutectoid rail					

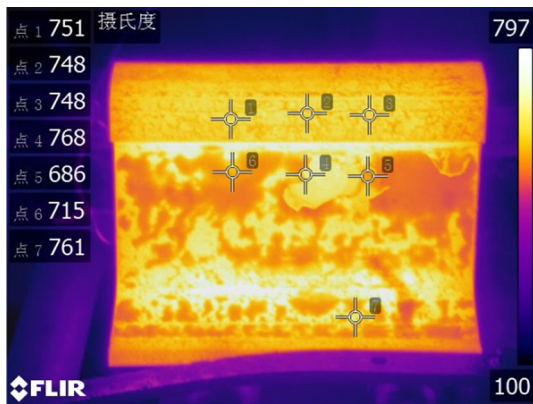


Figure 1 Infrared acquisition of rail quenching temperature.

more driving energy to cross the phase interface, thus reducing the crack growth rate.

Analysis of the fatigue crack growth rate of hypereutectoid rail

Paris formula under different cooling rates

When fatigue crack growth rate is constant, the relationship between da/dN and ΔK at the crack tip can be described by the classical Paris formula [13, 14]:

$$da/dN = C(\Delta K)^m \tag{1}$$

where da/dN is the fatigue crack growth rate, ΔK is the stress intensity factor range, and C and m are material parameters.

The $a-N$ curve in the previous section is derived and fitted, and the Paris formulas under five different quenching cooling rates are obtained. Figure 4 shows the $da/dN-\Delta K$ curve with cooling rates of 1 °C/s, 2 °C/s, 3 °C/s, 5 °C/s and 8 °C/s. Figure 4 shows that the da/dN increases with an increase in ΔK . However, different quenching cooling rates have the obvious different influences on the fatigue crack

growth rate of the samples. The crack growth rates with cooling rates of 1 °C/s, 2 °C/s, 3 °C/s, 5 °C/s and 8 °C/s are roughly equal at point P ($\Delta K = 13.5 \text{ MPa m}^{1/2}$). The crack growth rate of 8 °C/s is the smallest when $\Delta K < 13.5 \text{ MPa m}^{1/2}$. Based on the trends, it appears that the sample produced with the cooling rate of 8 °C/s would have a highest fatigue crack growth threshold ΔK_{th} , which indicates that the sample with a cooling rate of 8 °C/s would have a highest resistance for the crack initiation.

Effect of the quenching rate on fatigue crack growth

According to the requirements of the TB/T 2344-2012, the fatigue crack growth rate of da/dN is studied when the stress intensity factor range of $\Delta K = 10 \text{ MPa m}^{1/2}$ and $\Delta K = 13.5 \text{ MPa m}^{1/2}$. The values of stress intensity factor range, at any number of cycles, were calculated according to an equation of the GB/T6398-2000, and Origin 8.0 software was used for fitting the $a-N$ data and the derivatives of the $a-N$ curve on which the fatigue crack growth rates were calculated. The da/dN is shown in Table 4 when $\Delta K = 10 \text{ MPa m}^{1/2}$ and $\Delta K = 13.5 \text{ MPa m}^{1/2}$.

Table 4 shows that an increase in the cooling rate decreases the value C and increases m . In addition, the da/dN shows a decreasing trend at $\Delta K = 10 \text{ MPa m}^{1/2}$, the da/dN does not change much at $\Delta K = 13.5 \text{ MPa m}^{1/2}$ with the increase in cooling rate. While $\Delta K = 10 \text{ MPa m}^{1/2}$ or $\Delta K = 13.5 \text{ MPa m}^{1/2}$, the sample with a cooling rate of 8 °C/s has the lowest value C , the highest value m and the slowest fatigue crack growth rate. The sample with a cooling rate of 1 °C/s has the highest value C , the lowest value m and the fastest fatigue crack growth rate. These results shows that the sample with the cooling rate 1 °C/s is more sensitive to the stress intensity factor range at crack tip than the other samples at the crack growth stage; This conclusion is both similar and

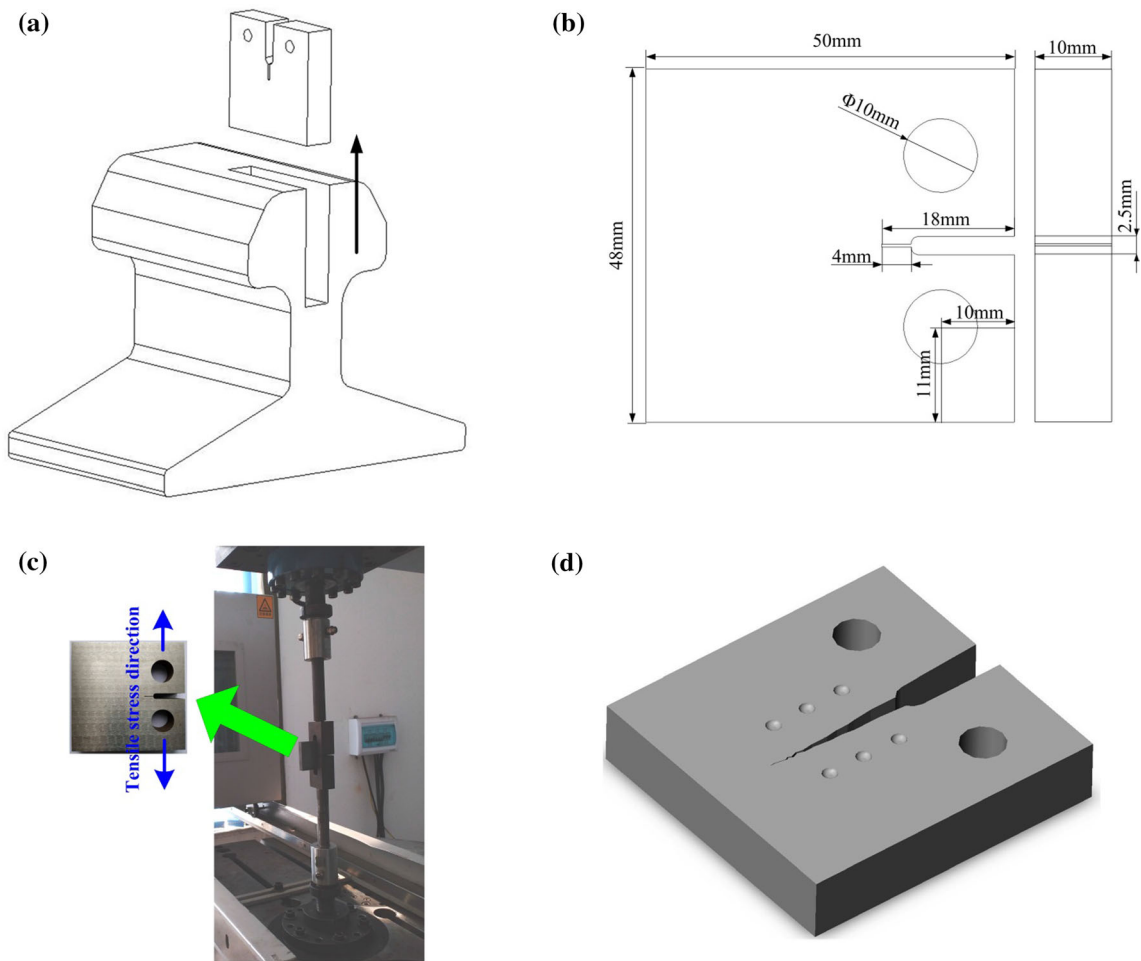


Figure 2 Sampling position and size of the CT sample: **a** sampling position and; **b** sample size; **c** fatigue test and **d** schematic diagram of hardness test location.

Table 3 Measurement of a and N with different quenching cooling rates

Cooling rate	1 °C/s	2 °C/s	3 °C/s	5 °C/s	8 °C/s
a (mm)	20.05	20.80	20.30	20.30	21.10
N (10^4 cycle)	70	77	79	94	106

consistent with the previous fatigue crack growth $a-N$ of this material.

Analysis of the fatigue crack growth mechanism

Effect of different quenching rates on hardness

Quenching is an effective way to increase the hardness, wear resistance and fatigue resistance of rail,

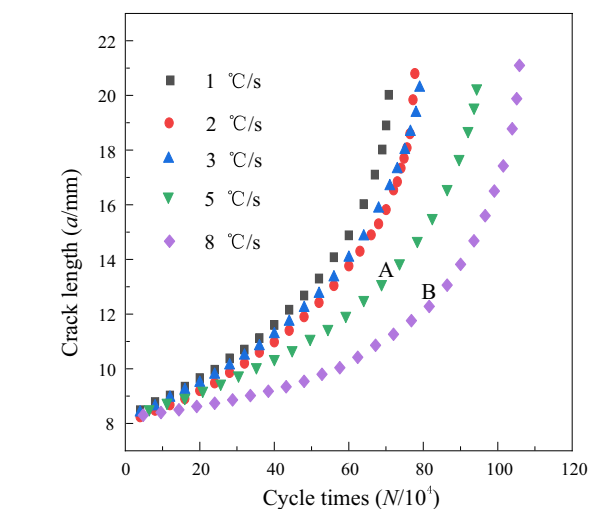


Figure 3 $a-N$ curve of hypereutectoid rail at different quenching rates.

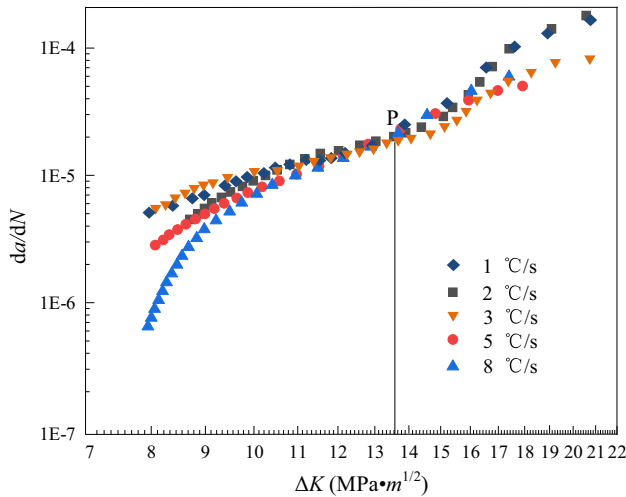


Figure 4 da/dN – ΔK curve with cooling rates of 1 °C/s, 2 °C/s, 3 °C/s, 5 °C/s and 8 °C/s.

and improve its lamellar structure [15]. Therefore, it is necessary to compare and analyze the hardness to explain the fatigue crack growth rate at different quenching rates. Table 5 shows the hardness of hypereutectoid rail under different cooling rates. It can be seen that the hardness of hypereutectoid rail increases with an increase in the cooling rate, the hardness of rail with an 8 °C/s cooling rate is the highest in all of the tests, which is beneficial to improve the wheel–rail wear.

Microstructure and crack growth path

The microstructure, strength, load and other factors of steel affect fatigue fracture morphology and the crack growth path [16]. To further study the effect of the quenching process on rail fatigue crack growth rate, the microstructure and fatigue fracture of hypereutectoid rail CT samples with different quenching rates were observed and analyzed using SEM.

Table 5 Hardness of hypereutectoid rail under different quenching rates

Cooling rate	1 °C/s	2 °C/s	3 °C/s	5 °C/s	8 °C/s
Hardness (HB)	316	326	335	346	392

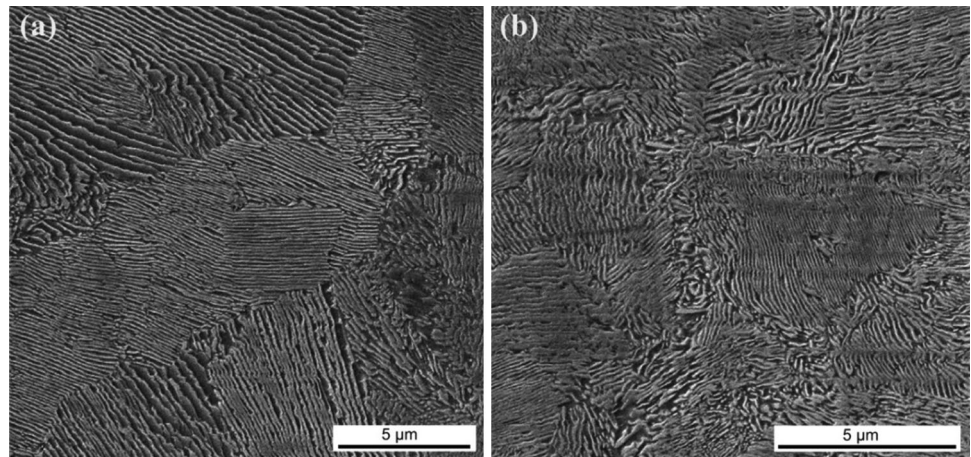
1. The effect of different quenching cooling rates on microstructure of hypereutectoid rail.

Pearlite structure is flake or granular at different quenching rates, while hypereutectoid rail steel with good properties needs a flake structure [17]. For hypereutectoid steel, the pearlite cluster diameter and pearlite lamellar spacing are important structural characteristics that influence fatigue crack growth performance. The representative samples with cooling rates of 2 °C/s and 8 °C/s were selected for analysis, and the SEM microstructure of hypereutectoid rail is shown in Fig. 5. The pearlite lamellae distance with cooling rates of 2 °C/s and 8 °C/s is 108.20 nm and 55.17 nm, and the cluster distance with cooling rates of 2 °C/s and 8 °C/s are 9 μm and 5.9 μm, respectively. For pearlitic steel, the mode of crack initiation and propagation in the pearlite depends on the orientation relationship between the lamellae and loading axis, and the size of the pearlite lamellae. When the specimen position and crack growth direction are known, the main factors determining the crack initiation and growth are the orientation of the pearlite lamellae and the size of the lamellar spacing. Because of the excellent plasticity of ferrite in the pearlite lamellae structure, the crack preferentially propagates in its interior, while the cementite lamellae are hard with dislocations that are difficult to pass through, thus forming dislocation pileups and impeding crack propagation. Therefore, finer lamellae spacing increases the number of

Table 4 Fatigue crack growth constant C , m and the crack growth rate

Cooling rate	$C/10^{-11}$	m	da/dN (m/Gc)	
			$\Delta K = 10 \text{ MPa m}^{1/2}$	$\Delta K = 13.5 \text{ MPa m}^{1/2}$
1 °C/s	2.597228	2.59469	10.3	22.2
2 °C/s	1.743282	2.79990	9.5	21.4
3 °C/s	0.870623	3.00447	8.7	22.0
5 °C/s	0.237012	3.51906	7.8	22.5
8 °C/s	0.116402	3.79305	7.2	22.5

Figure 5 SEM microstructure of hypereutectoid rail: **a** 2 °C/s cooling rate and **b** 8 °C/s cooling rate.



cementite lamellae and the effect of impeding crack propagation becomes more obvious.

- The fracture morphology of $\Delta K = 10 \text{ MPa m}^{1/2}$ of hypereutectoid rail.

The fatigue fracture SEM images of hypereutectoid rail under different cooling rates are shown in Fig. 6. It was found that there were significant differences on the fractographs of the samples with different quenching rates when $\Delta K = 10 \text{ MPa m}^{1/2}$. There are river patterns on the fatigue fracture surfaces in all of the samples. Figure 6a shows that the fracture surface of the sample with the cooling rate of 1 °C/s is

smooth and there is no branching crack. There are many river patterns and the fracture is a transgranular fracture. The formation of the river pattern is due to the fact that the crack propagation is not in a single plane. However, in the adjacent plane, a series of parallel and simultaneous cracks appear that will consume a certain amount of energy to form an additional propagation surface, so the river patterns tend to merge. Moreover, there are tearing steps on the fracture surface and fatigue striations on the tearing steps. Figure 6b shows that the fracture surface of the sample with the cooling rate of 2 °C/s is relatively smooth, is accompanied by obvious fatigue

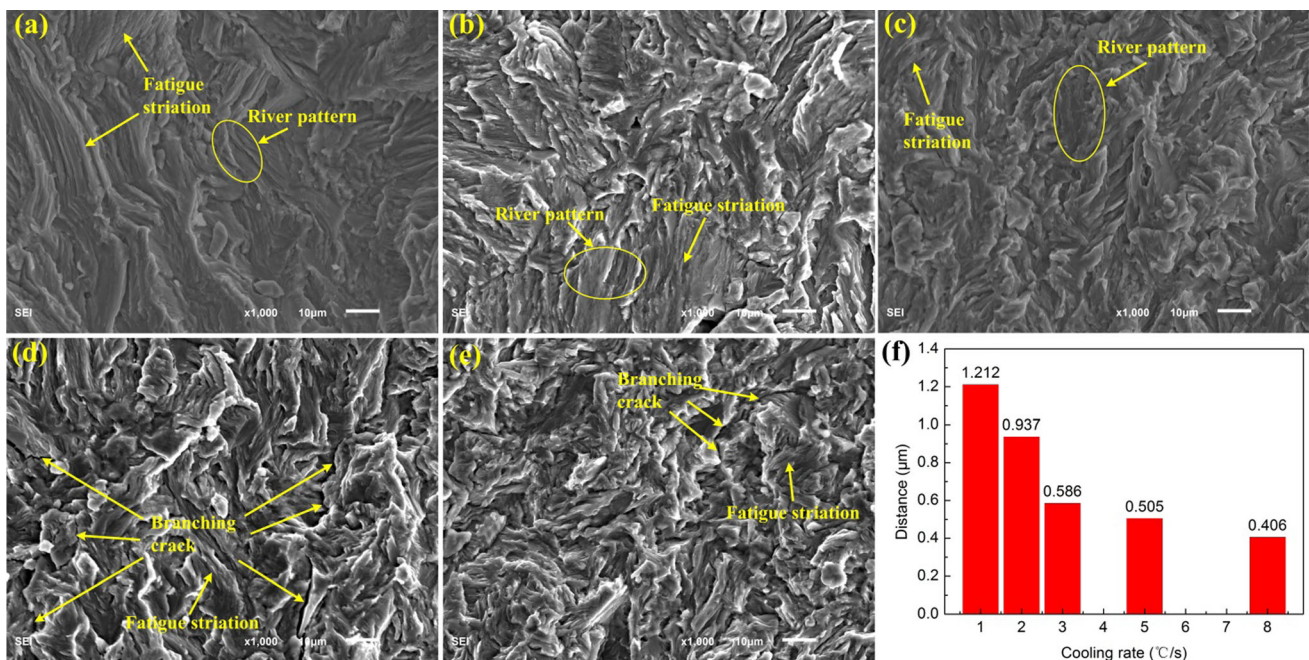


Figure 6 SEM fracture morphology when $\Delta K = 10 \text{ MPa m}^{1/2}$: **a** 1 °C/s cooling rate; **b** 2 °C/s cooling rate; **c** 3 °C/s cooling rate; **d** 5 °C/s cooling rate; **e** 8 °C/s cooling rate; and **f** fatigue striation spacing.

striation, and shows evidence of a large number of small fatigue striations within the small area, and that the fracture is a transgranular fracture. There are small tearing edges on the fracture surface, which are accompanied by river patterns. The number of river patterns is large, but the tributary is the main one and confluence of the tributaries is rare. Figure 6c shows that the fracture surface of the sample with a cooling rate of 3 °C/s is rougher than that of the sample with a cooling rate 1 °C/s, there are more facets and tearing edges, few fatigue striation, there are river patterns on the fracture surface, the number of river patterns is small, the steps are short and most of them are tributaries that rarely demonstrate confluence. Figure 6d, e shows that the fracture surfaces of the samples with cooling rates of 5 °C/s and / 8 °C/s are rough, exhibiting more tearing edges, bending, sharp and different directions of the tearing edges, and branching cracks on the surface. In addition, there are few fatigue striations. Figure 6f shows that the decreased fatigue striation spacing with an increase in cooling rate. The main reason for these results is that the crack growth is not only restricted by the state of the front edge of the crack tip, but it is also affected by the contact property of the crack surface at the back of the crack tip. It is known that rail under the stress of a crack tip has no favorable conditions for forming fatigue striations due to its high strength and small plastic deformation at the crack tip and adjacent area.

Figure 7 shows the fatigue crack growth path of hypereutectoid rail with cooling rates of 2 °C/s and 8 °C/s when $\Delta K = 10 \text{ MPa m}^{1/2}$. Figure 7 shows that the surface crack trend of the 2 °C/s cooling rate specimen is relatively straight, which corresponds to the smooth fracture; the rough fracture of the 8 °C/s cooling rate specimen corresponds to the zigzag crack growth path, which is related to the smaller

pearlite lamellar spacing and cluster diameter of the rail after quenching. This can be attributed to the fine pearlite lamellar spacing in cooling rate of 8 °C restrain the crack growth. The zigzag path and the zigzag fold back can consume more energy and release the stress at the crack tip, thereby reducing the crack growth rate when crack opening.

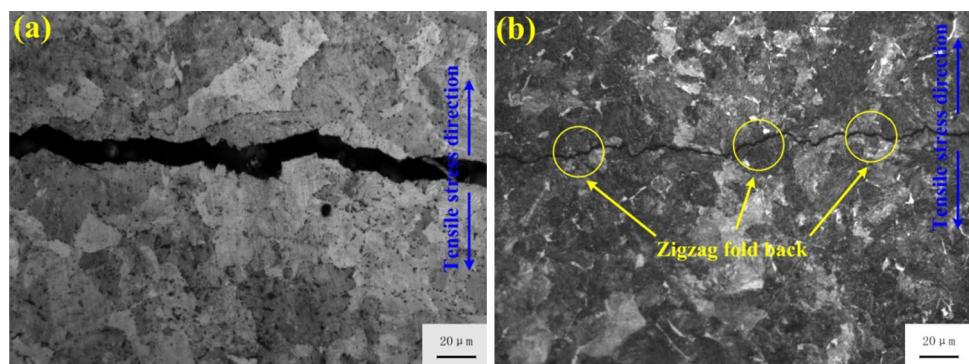
3. The fracture morphology of $\Delta K = 13.5 \text{ MPa m}^{1/2}$ of hypereutectoid rail.

The SEM images of the fatigue fracture of hypereutectoid rail under different cooling rates are shown in Fig. 8. It was found that there were no significant differences on the fractographs of the samples with different quenching rates when $\Delta K = 13.5 \text{ MPa m}^{1/2}$. There are branching cracks on the fatigue fracture surfaces in all of the samples. The general rule is that the crack always propagates along the weakest position in the material [18], and it is easiest to propagate along the boundary between the ferrite and pearlite. However, the pearlite lamellae are not always parallel to the crack propagation direction. Therefore, when the crack propagates along the boundary between the ferrite and pearlite, and meets the pearlite group boundary, the crack propagation is blocked, thereby changing its direction and leading to the production of branching cracks.

Figure 9 shows the fatigue crack growth path of hypereutectoid rail with cooling rates of 2 °C/s and 8 °C/s. Figure 9 shows that the surface crack growth path has significant turning and bifurcation characteristics when $\Delta K = 13.5 \text{ MPa m}^{1/2}$, and that the zigzag pattern is found in the both 2 °C/s and 8 °C/s cooling rate of hypereutectoid steel, but it is more obvious in the cooling rate 8 °C/s specimen. Branching cracks often occur in the large fold back because the crack growth at the fold back is blocked and the branching cracks will be generated in the

Figure 7 Crack growth paths when $\Delta K = 10 \text{ MPa m}^{1/2}$:

- a 2 °C/s cooling rate and
b 8 °C/s cooling rate.



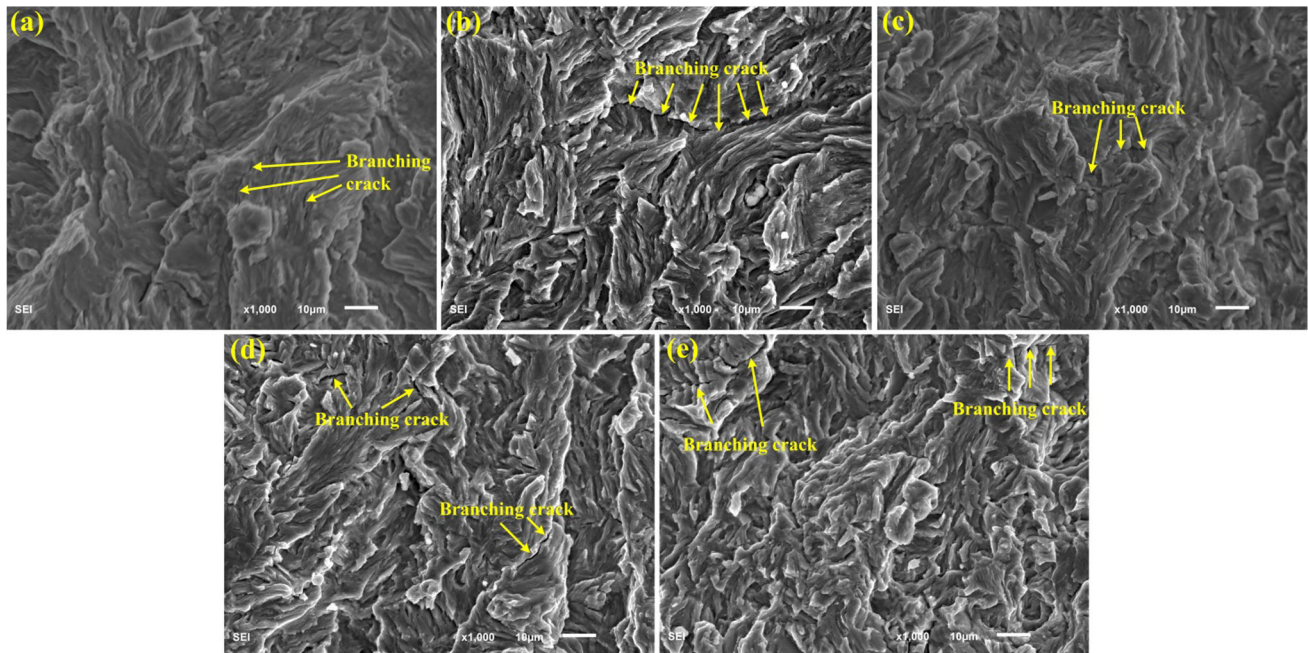
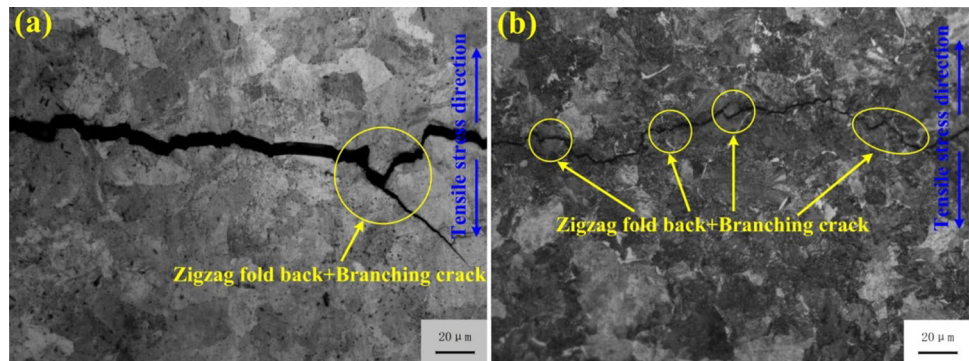


Figure 8 SEM fracture morphology when $\Delta K = 13.5 \text{ MPa m}^{1/2}$: **a** 1 °C/s cooling rate; **b** 2 °C/s cooling rate; **c** 3 °C/s cooling rate; **d** 5 °C/s cooling rate; **e** 8 °C/s cooling rate.

Figure 9 Crack growth path when $\Delta K = 13.5 \text{ MPa m}^{1/2}$: **a** 2 °C/s cooling rate and **b** 8 °C/s cooling rate.



stress concentration in order to release the stress. This kind of zigzag pattern will increase the total path of the crack growth, thereby reducing the crack growth rate. The back-break is reflected in an increase in the tearing edges, the depth of gullies in the river pattern and the rough surface of the fracture.

In summary, the fatigue crack growth rate is different under different quenching cooling rates and different values of ΔK . When the cooling rate is slow, the fatigue striation spacing was relatively larger, the area of river pattern is large, the tearing edge is shallow and the trend is single, and the surface is relatively smooth. When the cooling rate is fast, the fatigue striation spacing was relatively small, the area of river patterns is small, the tearing edges are deep

and the trend is variable, and the surfaces are relatively rough. This is related to the microstructure, and the pearlite lamellae and agglomerate distance of the 8 °C/s sample is smaller than that of the 2 °C/s sample. Because of the good plasticity of ferrite in the pearlite lamellae structure, the crack preferentially propagates in it, while the cementite lamellae is hard and the dislocation is difficult to pass through, thus forming dislocation pileups and hindering crack propagation. Therefore, the finer lamellae distance increases the number of cementite lamellae and hinders growth of the crack. In addition, the effect of the crack growth is more obvious, which makes the fracture rough. When crack growth meets the pearlite group, because of the different orientations of

cementite at the boundary of each pearlite group and the wide ferrite band, under the action of the stress at the crack tip, the crack will germinate and expand in the ferrite [19]. Moreover, due to the large differences of the mechanical properties between ferrite and cementite, the deformation is not homogeneous, and the stress concentration will occur at the interface of the ferrite and cementite; when the stress concentration exceeds the interface bonding strength, the crack can germinate and expand at the ferrite cementite interface. For the hypereutectoid steel with an 8 °C/s cooling rate, when the crack tip meets the cementite, the crack has to change its propagation direction such that the propagation path becomes a zigzag pattern and the crack propagation rate decreases.

Conclusions

The results of this research advance our understanding of the fatigue crack growth of rail, which is beneficial to restrain the fatigue crack growth rate, in three main areas.

1. With an increase in cooling rate, the Paris law parameters of C decreased, and m increased, the da/dN showed a decreasing trend with an increasing in cooling rate when the $\Delta K = 10 \text{ MPa m}^{1/2}$, and the da/dN did not change much with an increasing in cooling rate when the $\Delta K = 13.5 \text{ MPa m}^{1/2}$. The value C was the highest and the value m was the lowest in the 1 °C/s cooling rate specimen of hypereutectoid rail, and the fatigue crack growth rates were the fastest. In addition, the value C was the lowest and the value m was the highest in the 8 °C/s cooling rate specimen, and the fatigue crack growth rate was the slowest resulting in the best fatigue performance.
2. An increasing in the cooling rate resulted in a decrease in the lamellar spacing and cluster diameter of the pearlite. The lamellar spacing of the pearlite in cooling rates of 2 °C/s and 8 °C/s was 108.20 nm and 55.17 nm, respectively, and the cluster diameters of the pearlite were 9 μm and 5.9 μm, respectively. The smaller the lamellar spacing and cluster diameter, the easier the crack passed through the pearlite cluster boundary, which increased the number of zigzag crack growth paths and branching cracks. In addition, the number of cementite lamellae increased and the effect of restrained fatigue crack growth became more obvious.
3. The fatigue crack growth rate of hypereutectoid rail varied with different quenching cooling rates and different values of ΔK . The hypereutectoid rail with the cooling rate of 2 °C/s had many smooth facets of fatigue fracture, shallow gullies in the river pattern and a straight crack growth path. When the cooling rate was 8 °C/s, the fatigue fracture was rough, the area of river pattern was small, and the groove and the crack growth path showed a zigzag pattern, which is beneficial to restrain overall fatigue crack growth.

Acknowledgements

This work was supported by the Natural Science Foundation of Inner Mongolia (2019LH05016) and the Innovation fund of Inner Mongolia University of Science and Technology (2019QDL-B06).

Compliance with ethical standards

Conflict of interest The authors declare that they have no conflict of interest.

References

- [1] Zhang YH, Zhou QY, Bao L, Gao Y, Chen CY, Li C (2015) Comparative study on rail performance of high speed railway home and abroad. *China Railw Sci* 36:20–26
- [2] Guo HM, Wang WJ, Liu TF, Liu JH, Guo J, Liu QY (2014) Analysis of rail damage behavior of heavy haul railway. *China Mech Eng* 25:267–272
- [3] Zhou QY, Zhang JF, Guo ZW, Xi NS, Gao XP (2010) Research on the rail damages and the preventive countermeasures in heavy haul railways. *China Railw Sci* 31:27–31
- [4] Bao XR, Wang JA, Wang XD, Guo F, Liu YZ (2018) Effects of lanthanum on hot deformation behaviour of Mn–Cr–Mo bainitic rail steel. *J Rare Earths* 36:772–780
- [5] Li YG, Zhang FC, Chen C, Lv B, Yang ZN, Zheng CL (2016) Effects of deformation on the microstructures and mechanical properties of carbide-free bainitic steel for railway crossing and its hydrogen embrittlement characteristics. *Mat Sci Eng A Struct* 651:945–950
- [6] Zhou ZG (1990) Factors affecting the properties of quenched rails. *J China Railw Soc* 12:74–79

- [7] Gong S, Ren XC, Ma YX (2015) Effect of heat-treatment on microstructure and fracture toughness of high-speed railway wheel steel. *Trans Mater Heat Treat* 36:150–155
- [8] Akama M, Kiuchi A (2018) Fatigue crack growth under non-proportional mixed mode I/III loading in rail and wheel steel. *Tetsu to Hagane* 104:689–698
- [9] Jones R (2014) Fatigue crack growth and damage tolerance. *Fatigue Fract Eng Mater Struct* 37:463–483
- [10] Gao WL, Qin F, Jin T, Xie GZ (2017) Analysis of fatigue crack initiation and propagation on U71Mn steel rail during service. *J Hunan Univ Nat Sci* 44:25–29
- [11] Chen L, Chen KY, Chang G, Liu YY (2016) Effects of applied stress on isothermal phase transformation of austenite to pearlite in heavy rail steels: an experimental and modeling study. *Metallogr Microstruct Anal* 5:402–410
- [12] Chen L, Wang HJ, Guo FX (2017) Effect of quenching microstructure on fatigue crack growth rate of heavy rail steel. *Mater Rev* 31:109–112
- [13] Ma YJ, Youssef SS, Feng X, Wang H, Huang SS, Qiu JK, Lei JF, Yang R (2018) Fatigue crack tip plastic zone of $\alpha + \beta$ titanium alloy with widmanstatten microstructure. *J Mater Sci Technol* 34:2107–2115
- [14] Zhong ZH, Gu YF, Osada T, Yuan Y, Cui CY, Yokokawa T, Tetsui T, Harada H (2011) Fatigue crack growth characteristics of a new Ni–Co-base superalloy TMW-4M3: effects of temperature and load ratio. *J Mater Sci* 46:7573–7581. <https://doi.org/10.1007/s10853-011-5732-0>
- [15] Li J, Zhu LW, Zhu ZS, Wang XN (2014) Mathematical equations on fatigue crack growth rate of TC4-DT titanium alloy. *Titanium Ind Prog* 21:22–25
- [16] Dai PQ, He ZR, Mao ZY (2003) In situ TEM observation of crack initiation and propagation in pearlite. *Trans Mater Heat Treat* 24:41–45
- [17] Masoumi M, Sinatora A, Goldenstein H (2019) Role of microstructure and crystallographic orientation in fatigue crack failure analysis of a heavy haul railway rail. *Eng Fail Anal* 96:320–329
- [18] Jun HK, Seo JW, Jeon IS, Lee SH, Chang YS (2016) Fracture and fatigue crack growth analyses on a weld-repaired railway rail. *Eng Fail Anal* 59:478–492
- [19] Sun SH (2004) Effect of microstructure on propagation rate of fatigue crack in pearlitic steels. *MET Phys Exam Test* 30:7–10

Publisher's Note Springer Nature remains neutral with regard to jurisdictional claims in published maps and institutional affiliations.